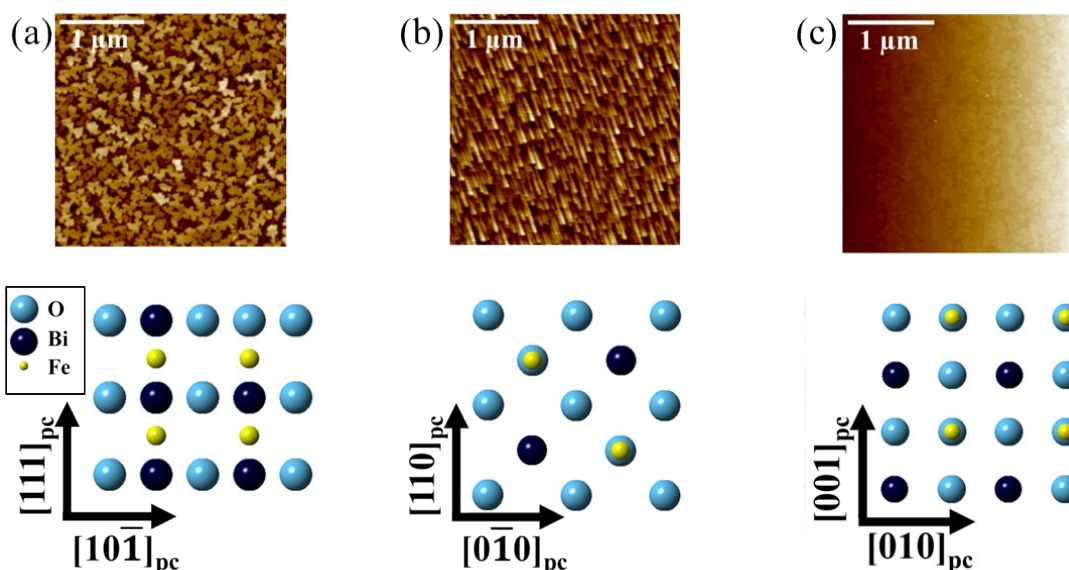
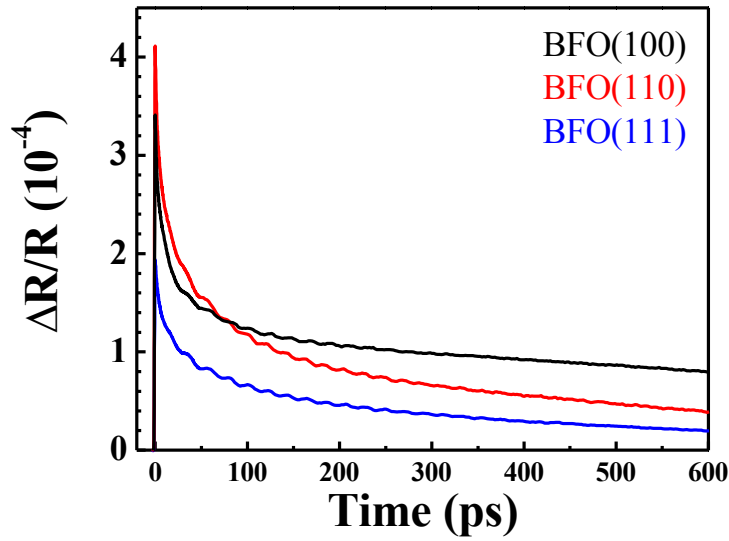


### Roughness issue:

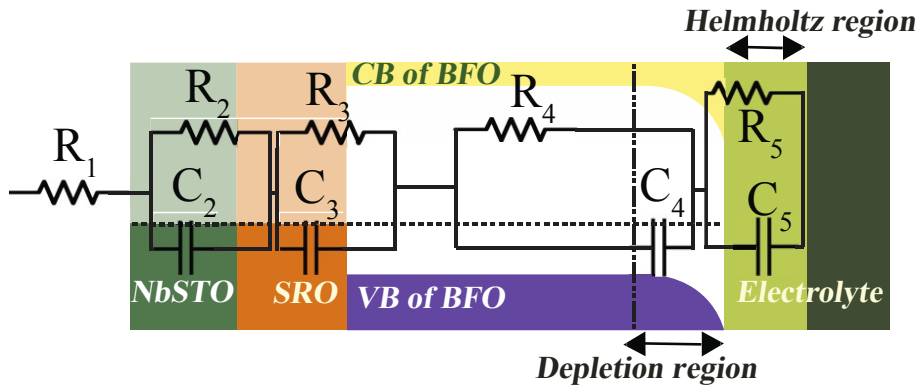
The surface area of the BFO films with various crystal orientations can be estimated with their surface roughness ( $R_a$ ) extracted from the AFM topographic images. Taking the case of BFO (111) film (with the largest roughness) as an example (Figure S1), tetrahedron shaped islands/plateaus form on the surface, which give extra surface from the side area. By depicting the contour of the islands on BFO (111) film, the extra surface area ( $\sim 0.14 \mu\text{m}^2$ ) can be estimated from the averaged perimeter of the islands/plateaus and the surface roughness ( $R_a=3.8 \text{ nm}$ ). Comparing to a perfectly flat surface ( $R_a=0 \text{ nm}$ ) with the same size ( $2 \mu\text{m}^2$ , shown in the following figure), the roughness of the sample only gives  $\sim 7\%$  extra surface area. The same approach has been used to calculate the surface area to be 26.2, 25.1, and  $25.0 \mu\text{m}^2$  for BFO (111), (110), and (100) samples in a scanning area of  $5 \mu\text{m}$  by  $5 \mu\text{m}$ , respectively. The surface area of BFO(111), the roughest one, is only  $\sim 4.8\%$  larger than that of BFO(100), the smoothest one. However, the photocurrent of BFO (111) film is more than 50% larger comparing to BFO (100) film. Thus, we concluded that the surface area is a minor factor in the anisotropic photoelectric behavior.



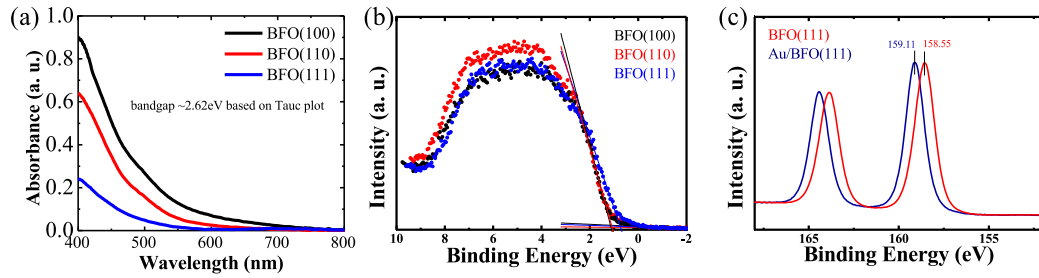
S1 Topography and schematic of crystal structure of *P*-up BFO thin film in three different orientations: (a) (111), (b) (110), and (c) (001). The roughness of average ( $R_a$ ): 3.8 nm, 1.1 nm, and 0.5 nm for (111), (110), and (001), respectively.



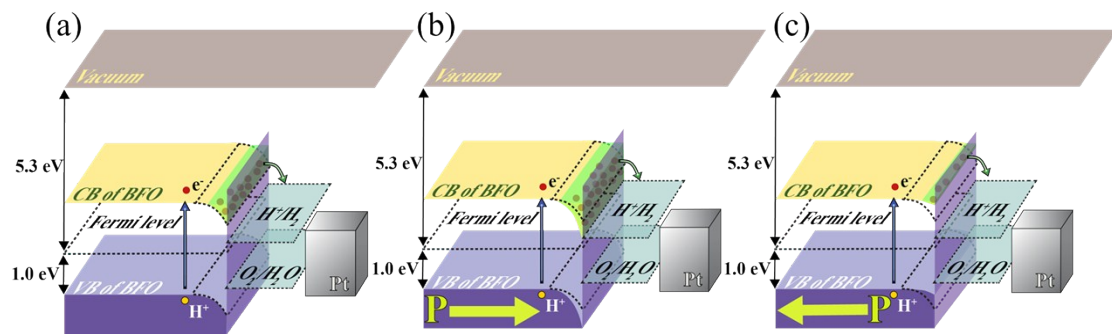
**S2.** The pump-probe analysis of three different orientations of *P*-up BFO thin films: This reveals the extreme short time scale (hundreds of ps) of electron dynamics in BFO.



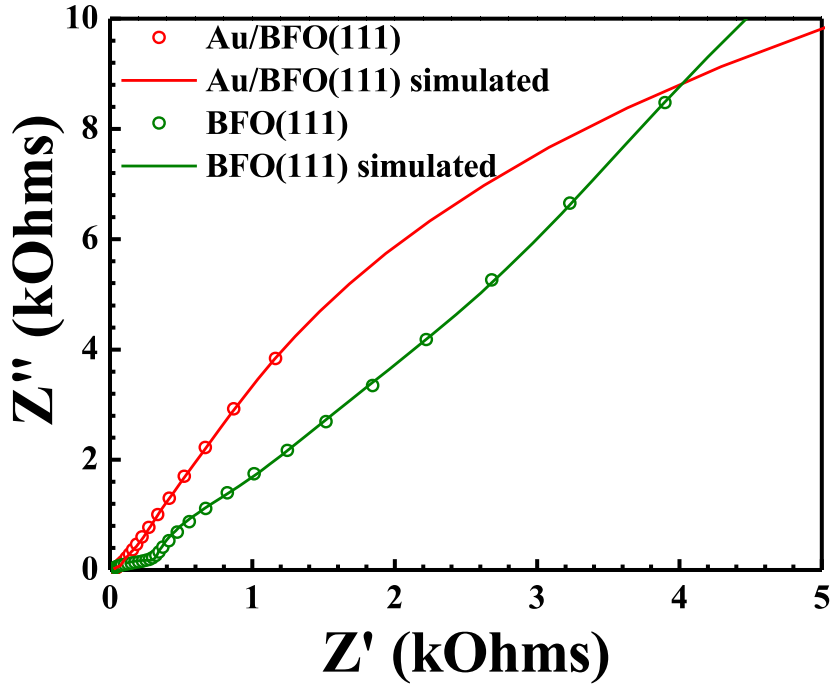
**S3.** The equivalent circuit model of charge transfer in photoelectrode.  $R_1$  is the connection resistance of external circuit and the resistance of substrate.  $R_2$  is the contact resistance between Nb-STO and its bottom electrode and  $C_2$  represents the capacitance induced by interface defects between Nb-STO and its bottom electrode.  $R_3$  is the contact resistance between BFO and its bottom electrode and  $C_3$  represents the capacitance induced by interface defects between BFO and its bottom electrode.  $R_4$  is the resistance of charge transfer in BFO and  $C_4$  is the capacitance in depletion region in BFO.  $R_5$  is the resistance of charge transfer from BFO to electrolyte and  $C_4$  is responsible for the capacitance of Helmholtz region in electrolyte.



**S4** (a) Optical absorption of three orientations of *P*-up BFO thin films. (b) Ultraviolet photoelectron spectroscopy (UPS) is utilized to reveal the energy between the valence bands maximum to the Fermi level of the *P*-up BFO films in three different orientations. The positions of the valence band maximum were obtained by the intersection of background and the linear fit. (c) High resolution x-ray photoelectron spectroscopy (XPS) is utilized to unveil the core level electronic structure of the *P*-up BFO and Au/BFO samples.



**S5** Schematic of ferroelectric field effect on depletion region at the interface of BFO and water. (a) Non-polar BFO. (b) Schematic of BFO with spontaneous upward polarization. (c) Schematic of BFO with spontaneous downward polarization. The dash line indicates the band bending in non-polar BFO as reference. (take out-of-plane direction as up).

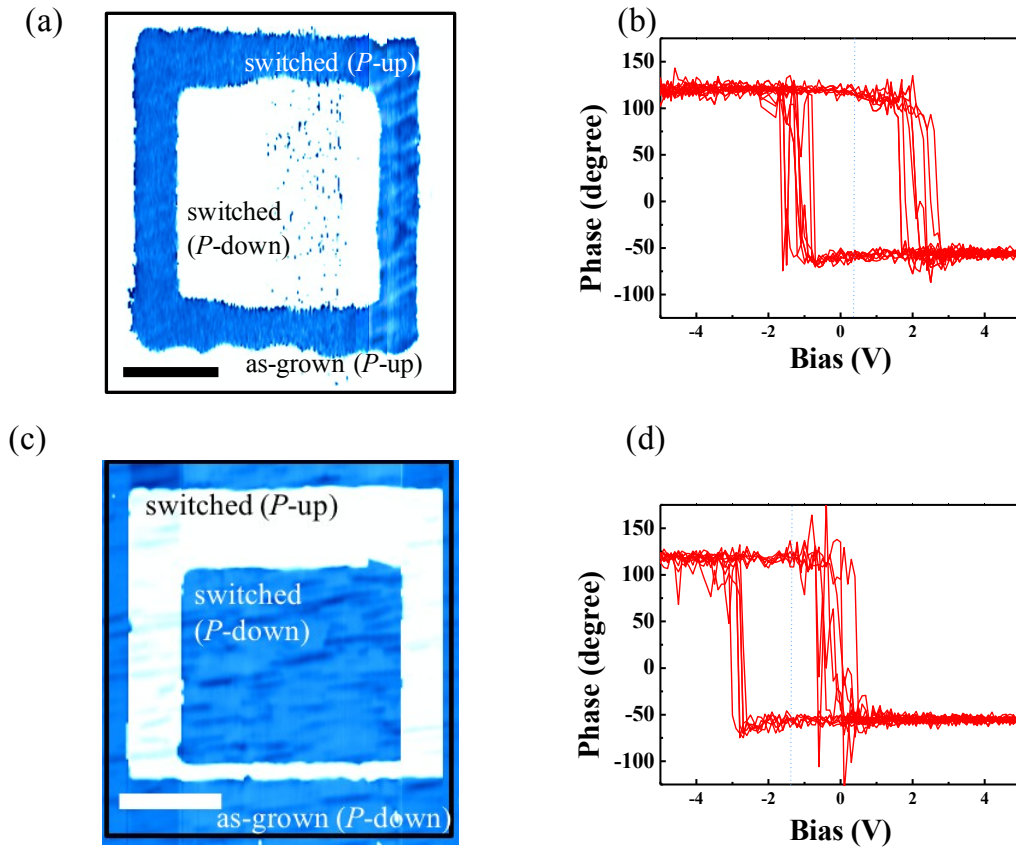


**S6.** Electrochemical impedance spectroscopic analysis of Au/BFO(111) and BFO(111).

**The polarization in as-grown state and ferroelectricity:**

The self-poled feature and good ferroelectricity of our samples can be supported by the sharp contrast between the opposite polarizations in the PFM images (Figure S7(a) and (c)) as well as the presence of square hysteresis loops during the ferroelectric switching process (Figure S7(b) and (d)). To distinguish the polarization direction in the as-grown state, we applied different DC bias on the Pt coated tip with the samples grounded. Take Figure S7(a) for example, firstly +7V was applied via the tip and scanned an area of  $3\mu\text{m}$  by  $3\mu\text{m}$ , then applied -7V was applied and scanned an area of  $2\mu\text{m}$  by  $2\mu\text{m}$  on the sample. After the application of DC bias, we employed the AC signal through the tip with the peak-to-peak amplitude of 2V and the frequency of  $\sim 275\text{kHz}$ , the contrast in Figure S7(a) shows the  $180^\circ$  difference in phase, indicating the polarization in the area outside the switched boxes is pointing upward. The same approach can be used to examine the samples with down polarized state. Moreover, the clear shifts of the hysteresis loops (shown in Figure S7(b) and (d)) indicate the preference of the polarization direction in our samples. Typically, the *P*-up samples can be switched under the smaller negative tip bias and the *P*-down samples can be switched under the smaller positive tip bias. Overall, from the PFM phase images and

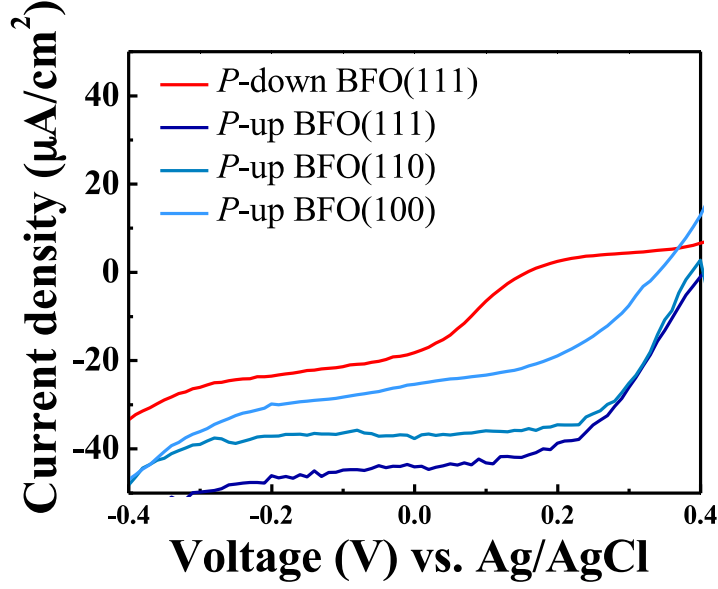
the ferroelectric switching loops, the evidence on the self-poling effect of our samples is demonstrated.



**S7.** Ferroelectric polarization switching. Out-of-plane PFM images (a) *P*-up BFO. (c) *P*-down BFO. The scale bar is 1  $\mu\text{m}$ . Typical hysteresis loops (b) *P*-up BFO (d) *P*-down BFO.

### **I-V measurements:**

The photocurrent density at zero bias of BFO is influenced by the polarization direction and crystal orientations. As shown in Figure S8, for the *P*-down BFO sample, the onset potential is 0.16 V and for the *P*-up BFO samples, the onset potentials are 0.41, 0.38, and 0.34 V, for (111), (110), and (100) respectively.



S8. The  $I$ - $V$  curves of the BFO films with different orientations and polarizations.

	$R_1$ ( $\Omega$ )	$R_2$ ( $\Omega$ )	$C_2$ ( $\mu\text{F}$ )	$R_3$ ( $\Omega$ )	$C_3$ ( $\mu\text{F}$ )	$R_4$ ( $\text{k}\Omega$ )	$C_4$ ( $\mu\text{F}$ )	$R_5$ ( $\text{k}\Omega$ )	$C_5$ ( $\mu\text{F}$ )
<b>Au/BFO (111)</b>	24.9	52	1.08	156	6.11	0.5	13.79	26.5	4.27
<b>BFO(111)</b>	58.8	260	1.42	809	0.008	2.1	3.15	59.8	2.02

Table S1. The fitting results of S6.

	$A_{10}$ ( $10^{-5}$ )	$\tau_{10}$ (ps)	$A_{100}$ ( $10^{-5}$ )	$\tau_{100}$ (ps)	$y_0$ ( $10^{-5}$ )
<b>BFO(100)</b>	13.068	11.7	8.261	185.0	7.983
<b>BFO(110)</b>	14.487	12.2	15.832	150.4	4.089
<b>BFO(111)</b>	6.632	13.5	8.558	180.6	1.854

**Table S2.** The fitting results of S2. These results are extracted by the following formula, where  $\Delta R/R$  is transient reflectivity change,  $A_{10}$  is the amplitude of decay time around 10 ps,  $\tau_{10}$  is the decay time around 10 ps, and  $A_{100}$  is the amplitude of decay time larger than hundreds of ps,  $\tau_{100}$  is the decay time larger than hundreds of ps.

$$\Delta R/R = A_{e-ph} e^{-t/\tau_{e-ph}} + A_{spin} e^{-t/\tau_{spin}} + y_0$$

